Original research article

The Study of the Intensity-Curvature Term: Applications in Magnetic Resonance Imaging of the Human Brain

Carlo Ciulla*
University of Information Science and Technology "St. Paul the Apostle"
Faculty of Information Systems Multimedia Visualization and Animation, Partizanska BB, 6000 Ohrid, Republic of Macedonia

Ustijana Rechkoska Shikoska
University of Information Science and Technology "St. Paul the Apostle"
Faculty of Computer Science and Engineering, Partizanska BB, 6000 Ohrid, Republic of Macedonia

Vasko Reckoski
University "St. Clement Ohridski", FTU, "Kej Makedonija" 95, 6000 Ohrid, Republic of Macedonia

Dimitar Veljanovski
Skopje City Hospital 8-mi Septemvri, Boulevard 8th September, Department of Diagnostic Radiology, 1000 Skopje, Republic of Macedonia

Filip A. Risteski
Skopje City Hospital 8-mi Septemvri, Boulevard 8th September, Department of Diagnostic Radiology, 1000 Skopje, Republic of Macedonia

Received 16 July 2016; Received in revised form 15 October 2016
Accepted 17 October 2016; Available online 24 March 2017

ABSTRACT

This paper presents an overview of the characteristics of the intensity-curvature term with applications in image processing and also in Magnetic Resonance Imaging (MRI) of the human brain. The intensity-curvature term is the key concept that merges together the value of the signal with the value of the classic-curvature, which is the sum of the second order partial derivatives of the model function fitted to the signal. The model function fitted to the signal needs to have the property of second order differentiability, and also to have at least one non null second order partial derivative calculated at the origin of the coordinate system of the pixel. The mathematical meaning of the intensity-curvature term is the mapping of the signal into a novel domain where each value of the signal is multiplied by the arctangent of the angle subtended with the horizontal, by the tangent to the first order derivative of the model function. The mapping merges the value of the signal intensity and the classic-curvature of the signal. Hence, the resulting intensity-curvature term embeds information about both signal intensity and concavity-convexity of the model function. In addition to the classic-curvature, and consequential to the mapping, the intensity-curvature term allows the calculation of three

***Corresponding author:** cxc2728@njit.edu **doi:** 10.14456/tijsat.2017.4

supplementary intensity-curvature measurement approaches (ICMAs): (i) the intensity-curvature functional, (ii) the signal resilient to interpolation, and (iii) the resilient curvature. This paper reviews the implications of the intensity-curvature term with specific focus on the meaning and the nature of the ICMAs, which provide additional imaging of the human brain MRI.

Keywords: Intensity-curvature term; Intensity-curvature measurement approaches; Classic-curvature; Intensity-curvature functional; Signal resilient to interpolation; Resilient curvature

Introduction

The literature

Feature extraction from Magnetic Resonance Imaging (MRI) data is not new. Indeed, a wide array of studies have been motivated to process the MRI data with the specific purpose to extract characteristics of the image intensity. The classification of tumor type and grade has been conducted using support vector machine automated classification paradigms after the extraction from MRI data of tumor shape and intensity characteristics [1]. MRI feature extraction is a useful task also when correlating with the complementary information from other imaging modalities like Computerized Tomography (CT) and Single Photon Emission Computerized Tomography (SPECT) [2]. Voxel wise comparison of multiple MRI data sets is the basis for voxel-based morphometry (VBM) which has been used to select voxels of interest to be used to detect Alzheimer's disease [3]. Feature extraction is also useful to MRI segmentation of specific structures such as the cingulum [4]. A support vector machine (SVM) approach to the classification of Alzheimer's disease patients, versus normal control subjects, made use of features extracted from MRI in order to represent gray matter, white matter and cerebrospinal fluid [5]. MRI signal intensity feature extraction is paramount in order to achieve human brain tissue recognition and identification [6]. Feature extraction from MRI images of the human brain can also be attained through the use of wavelets [7-9]. In addition to the aforementioned literature, also the intensity-curvature measurement approaches (ICMAs) have the capability to perform feature extraction from two-dimensional MRI images [10]. Using the properties of the ICMAs, this paper addresses the task of feature extraction from 2D images with applications in Magnetic Resonance Imaging of the human brain and more generally in image processing. The novelty of this research consists in reporting for the first time the study of the intensity-curvature term and also additional evidence related to the properties of the intensity-curvature measurement approaches. The intensity-curvature term is the concept that allows the calculation of three ICMAs in addition to the classic-curvature. On the basis of the empirical evidence, the classic-curvature (CC) and the intensity-curvature functional (ICF) were suggested to be high pass filtered MRI signals [11]. Further study is reported here to elucidate that the Fourier properties of the CC and the ICF are not the same. Moreover, this study reports that the Fourier properties of the MRI high pass filtered signal are different from the Fourier properties of the CC and the ICF. The signal resilient to interpolation is here confirmed to be an alternative filtering technique, and the resilient curvature is characterized as the image processing tool able to smooth, to invert and to magnify the gray scale of the image [12].

The intensity-curvature term

The key concept at the basis of the theoretical development of the intensity-curvature measurement approaches (ICMAs) is the intensity-curvature term [13]. This

paper addresses the explanation of the meaning of the intensity-curvature term: the product between: (i) the signal intensity and (ii) the arctangent of the angle subtended with the horizontal by the tangent to the first order derivative of the model function fitted to the image data. See chapter 1 in [14]. The classic-curvature embeds in itself the geometrical meaning of the arc subtended by the tangent to the first order derivative curve of the model function fitted to the signal. For simplicity an illustration of the concept in the case of unidimensional signal will be presented. In Fig. 1, the radius of the circle is *r*, and the value of the signal intensity is termed *I*. The tangent to the first order derivative curve is termed τ, the arc subtended, with the horizontal, by the tangent to the first order derivative curve is termed *a*. Thus, the geometrical meaning of the intensity-curvature term is the product $I \cdot a$. For values of the angle θ inside the open interval $| -\pi/2, \pi/2 |$, the multiplication of *a* times *I* results either in a reduction of *I* (when a = arc tang $(\theta) < 1$), or in a magnification of *I* (when a = arc tang $(\theta) > 1$), or in the same *I* (when $a = 1$). It follows that the signal *I* is mapped to the domain $I \cdot a$. At each time the signal is sampled, both *I* and *a* do change. To make explicit the math formulation of the intensity-curvature term we can rely on the constraint that *I* is equal to the radius (*r*) of the circle (see Fig. 1).

From the constraint it follows the generalization, which, for a diverse sampled *I*, considers always $I = r$. Since $a = r \cdot e^{i\theta} = r \cos(\theta) + r \sin(\theta)$, it follows that $I \cdot a = I \cdot [I \cos(\theta) + I \sin(\theta)]$. Thus, the rational flow implies that for given I = r and τ, the values of the angle θ and the length of the arc *a* are calculated, so to map *I* to $I \cdot [I \cos(\theta) + I \sin(\theta)]$. However, when calculating the product $I \cdot [I \cos(\theta) + I \sin(\theta)]$ (with $\theta = 2 \cdot \pi \cdot CC$; where CC is the classic-curvature), no meaningful image was obtained.

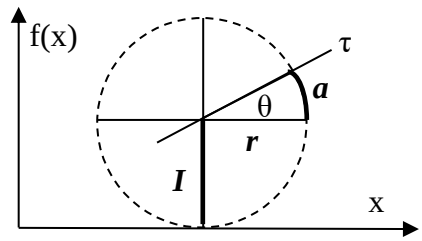

Fig. 1. The meaning of the intensity-curvature term: the signal *I* is mapped to the domain $I \cdot a$.

Thus, the *intensity-curvature terms* are: (i) the intensity-curvature term before interpolation E_0 [14], which is computed as the product of the signal intensity *I* times the classic-curvature calculated at the origin of the pixel. And, (ii) the intensity-curvature term after interpolation E_{IN} [14], which is computed as the product between the model function, and the classic-curvature calculated at the generic intra-pixel coordinate. Section 2 reports the formulae of E_0 and E_{IN} for the three polynomial functions used in this study.

Theory

The bivariate cubic formula

Let us consider the bivariate formula [10, 11, 15]:

$$f(x, y) = f(0, 0) + \phi_a (a x^2 + y) + \phi_b (b y^2 - x) + \phi_{ab} (a x^2 y + b y^2 x) \quad (1)$$

Let us posit:

$$\phi_a = [f(1, 0) - f(0, 0)] \quad (2)$$
$$\phi_b = [f(0, 1) - f(0, 0)] \quad (3)$$
$$\phi_{ab} = [f(1, 1) + f(0, 0) - f(0, 1) - f(1, 0)] \quad (4)$$

Where f(1, 1), f(0, 1), f(1, 0) are the neighboring pixels of f(0, 0), which is the pixel to recalculate. The classic-curvature of f(x, y) is:

$Y_C(x, y) = (\partial^2 f(x, y) / \partial x^2) + (\partial^2 f(x, y) / \partial y^2) + (\partial^2 f(x, y) / \partial x \partial y) + (\partial^2 f(x, y) / \partial y \partial x)$

$= \phi_a(2a) + \phi_{ab}(2ay) + \phi_b(2b) + \phi_{ab}(2bx) + 2\,\phi_{ab}(2a\,x + 2b\,y)$ (5)

The intensity-curvature terms before ($E_0(x, y)$) and after ($E_{IN}(x, y)$) interpolation are given by the solution of equations (6) and (7) [14].

$E_0(x, y) = \int\int f(0, 0) \cdot [\, Y_C(x, y)\,]_{(0, 0)}\, dxdy =$

$f(0, 0) \cdot \{\, \phi_a(2a) + \phi_b(2b)\,\} \cdot xy$ (6)

$E_{IN}(x, y) = \int\int f(x, y) \cdot [\, Y_C(x, y)\,]_{(x, y)}\, dxdy =$

$\{\, f(0, 0) \cdot H(x, y)\,\} + B(x, y) + C(x, y) + D(x, y)$ (7)

With the following positions:

$H(x, y) = \{\phi_a(2a\,xy) + \phi_{ab}(a\,xy^2) + \phi_b(2b\,xy) + \phi_{ab}(b\,x^2y) + 2\,\phi_{ab}(a\,x^2y + b\,xy^2)\}$ (8)

$B(x, y) = \{\phi_a(a\,x^3y/3 + xy^2/2) \cdot \phi_a(2a)\} + \{\phi_a(a^2\,x^3y^2/3 + a\,xy^3 \cdot (2/3)) \cdot \phi_{ab}\} + \{\phi_a(a\,yx^3/3 + xy^2/2) \cdot \phi_b(2b)\} + \{\phi_a(ab\,yx^4/2 + b\,x^2y^2/2) \cdot \phi_{ab}\} + \{\phi_a(a^2\,yx^4/2 + a\,x^2y^2/2 + ab\,x^3y^2/3 + b\,xy^3 \cdot (2/3)) \cdot 2\,\phi_{ab}\}$ (9)

$C(x, y) = \{\phi_b(b\,xy^3/3 - yx^2/2) \cdot \phi_a(2a)\} + \{\phi_b(ab\,xy^4/2 - a\,x^2y^2/2) \cdot \phi_{ab}\} + \{\phi_b(b\,xy^3/3 - x^2y/2) \cdot \phi_b(2b)\} + \{\phi_b(b^2\,x^2y^3/3 - b\,yx^3 \cdot (2/3)) \cdot \phi_{ab}\} + \{\phi_b(ab\,x^2y^3/3 - a\,yx^3\,2/3 + b^2\,xy^4/2 - b\,x^2y^2/2) \cdot 2\,\phi_{ab}\}$ (10)

$D(x, y) = \{\phi_{ab}(a\,x^3y^2/6 + b\,y^3x^2/6) \cdot \phi_a(2a)\} + \{\phi_{ab}(a^2\,x^3y^3\,2/9 + ab\,y^4x^2/4) \cdot \phi_{ab}\} + \{\phi_{ab}(a\,x^3y^2/6 + b\,y^3x^2/6) \cdot \phi_b(2b)\} + \{\phi_{ab}(ab\,x^4y^2/4 + b^2\,y^3x^3\,2/9) \cdot \phi_{ab}\} + \{\phi_{ab}(a^2\,x^4y^2/4 + ab\,y^3x^3 \cdot (2/9) + ab\,x^3y^3\,2/9 + b^2\,y^4x^2/4) \cdot 2\,\phi_{ab}\}$ (11)

The bivariate cubic Lagrange polynomial

Let us consider the bivariate cubic Lagrange interpolation formula [10, 12]:

$g_4(x, y) = f(0, 0) + \alpha_2 \cdot a\,[(x + y)^3 + (1/2)(x + y)^2 + (1/4)(x + y) + 1] + \alpha_3 \cdot a\,[(x + y)^2 + 2(x + y) + 1]$ (12)

Where α_2 and α_3 group together the pixels in the neighbor of f(0, 0), which is the pixel to recalculate.

$\alpha_2 = [f(1/2, 1/2) + f(-1/2, -1/2) + f(2/3, 2/3) + f(-2/3, -2/3) + f(-1, -1) + f(1, 1) + f(3/2, 3/2) + f(-3/2, -3/2)]$ (13)

$\alpha_3 = [f(1/2, 1/2) + f(-1/2, -1/2) + f(-1, -1) + f(1, 1)]$ (14)

The classic-curvature of $g_4(x, y)$ is:

$\Omega_C(x, y) = 4 \cdot \{\alpha_2 \cdot a\,[6(x + y) + 1] + 2\,\alpha_3 \cdot a\}$ (15)

The intensity-curvature terms before ($E_0(x, y)$) and after ($E_{IN}(x, y)$) interpolation are given by the solution of equations (16) and (17) [10, 12, 14].

$$E_0(x, y) = \int\int f(0, 0) \cdot [\ \Omega_C(x, y)\ ]_{(0, 0)}\ dxdy =$$

$$f\,(0, 0) \cdot 4 \cdot \{\ \alpha_2 \cdot a + 2\ \alpha_3 \cdot a\ \} \cdot xy \qquad (16)$$

$$E_{IN}(x, y) = \int\int g_4(x, y) \cdot [\ \Omega_C(x, y)\ ]_{(x, y)}\ dxdy$$

$$= 4 \cdot \{\ f\,(0, 0)\ \{\ \alpha_2 \cdot a\ [6\ (yx^2/2 + xy^2/2) +$$

$$xy] + 2\ \alpha_3 \cdot a\ xy\} + 6\ \varphi_4\ (\alpha_2\ a)^2 + \varphi_3\ [4\ (\alpha_2$$

$$a)^2 + 8\ \alpha_3\ \alpha_2\ a^2] + \varphi_2\ [2\ (\alpha_2\ a)^2 + 14\ \alpha_3\ \alpha_2\ a^2 +$$

$$2\ (\alpha_3\ a)^2] + \varphi_1\ [(25/4)\ (\alpha_2\ a)^2 + (17/2)\ \alpha_3\ \alpha_2$$

$$a^2 + 4\ (\alpha_3\ a)^2] + [(\alpha_2\ a)^2 + 3\ \alpha_3\ \alpha_2\ a^2 + 2\ (\alpha_3$$

$$a)^2]\ xy\} \qquad (17)$$

With the following positions:

$$\varphi_1 = [(1/2)\ yx^2 + (1/2)\ xy^2] \qquad (18)$$

$$\varphi_2 = [(1/3)\ yx^3 + (1/2)\ x^2y^2 + (1/3)\ xy^3] \qquad (19)$$

$$\varphi_3 = [(1/4)\ yx^4 + (1/2)\ x^3y^2 + (1/2)\ x^2y^3 +$$

$$(1/4)\ xy^4)] \qquad (20)$$

$$\varphi_4 = [(1/5)\ yx^5 + (1/2)\ x^4y^2 + (2/3)\ x^3y^3 +$$

$$(1/2)\ x^2y^4 + (1/5)\ xy^5] \qquad (21)$$

The signal resilient to interpolation f(0, 0) is calculated solving the equation $E_o(x, y) = E_{IN}(x, y)$ in f(0, 0) hereto follow.

$$f(0, 0) = \Delta_{LGR} / \Theta_{LGR} \qquad (22)$$

$$\Lambda_{LGR} = 6\ \varphi_4\ (\alpha_2\ a)^2 + \varphi_3\ [4\ (\alpha_2\ a)^2 + 8\ \alpha_3\ \alpha_2$$

$$a^2] + \varphi_2\ [2\ (\alpha_2\ a)^2 + 14\ \alpha_3\ \alpha_2\ a^2 + 2\ (\alpha_3\ a)^2] +$$
$$\varphi_1\ [(25/4)\ (\alpha_2\ a)^2 + (17/2)\ \alpha_3\ \alpha_2\ a^2 + 4\ (\alpha_3$$
$$a)^2] + [(\alpha_2\ a)^2 + 3\ \alpha_3\ \alpha_2\ a^2 + 2\ (\alpha_3\ a)^2]\ xy \qquad (23)$$

$$\Theta_{LGR} = [\alpha_2\ a + 2\ \alpha_3\ a]\ xy - \{\alpha_2 \cdot a\ [6\ (yx^2/2 +$$
$$xy^2/2) + xy] + 2\ \alpha_3 \cdot a\ xy\} \qquad (24)$$

The resilient curvature [12, 14] is calculated as the sum of second order partial derivatives of the signal resilient to interpolation:

$$RC(x, y) = (\partial^2\ (\ f(0, 0)\ )\ /\partial x^2) + (\partial^2\ (\ f(0, 0))$$

$$/\partial y^2) + (\partial^2\ (\ f(0, 0)\ )\ /\partial x \partial y) + (\partial^2\ (\ f(0, 0)\ )$$

$$/\partial y \partial x) \qquad (25)$$

The bivariate linear function

Let h be a continuous function that takes the form [11, 13, 15, 16].

$$h(x, y) = f(0,0) + x\ \theta_x + y\ \theta_y + xy\ \omega_f \qquad (26)$$

Where: f(0,0), f(1,0), f(0,1) and f(1,1) are the values of intensity at the four corners of the pixel. Such h(x, y) is the bivariate linear interpolation function. Let us posit:

$$\theta_x = [f(1,0) - f(0,0)] \qquad (27)$$
$$\theta_y = [f(0,1) - f(0,0)] \qquad (28)$$
$$\omega_f = [f(1,1) + f(0,0) - f(0,1) - f(1,0)] \qquad (29)$$

The classic-curvature of h(x, y) is:

$$\Psi_C(x, y) = 2\ \omega_f \qquad (30)$$

The intensity-curvature terms before interpolation ($E_0(x, y)$) and after interpolation ($E_{IN}(x, y)$) are given in equations (31) and (32) [11, 15, 16].

$$E_0(x, y) = \int\int f(0, 0) \cdot [\ \Psi_C(x, y)\ ]_{(0, 0)}\ dxdy =$$

$$f\,(0, 0)\ 2\ x\ y\ \omega_f \qquad (31)$$

$$E_{IN}(x, y) = \int\int h(x, y) \cdot [\ \Psi_C(x, y)\ ]_{(x, y)}\ dxdy$$

$$= 2\ \omega_f\ H_{xy}\,(x, y) \qquad (32)$$

With the position:

$$H_{xy}\,(x, y) = f(0,0)\ xy + yx^2/2\ \theta_x + xy^2/2\ \theta_y +$$

$$y^2x^2/4\ \omega_f \qquad (33)$$

The intensity-curvature functional of h(x, y) is:

$$\Delta E(x, y) = E_o(x, y) / E_{IN}(x, y) \quad (34)$$

Results

Study of the intensity-curvature terms of theoretical images

This section of the paper presents the images of the intensity-curvature terms calculated using theoretical images. The terminology: 'before interpolation', and 'after interpolation' does not imply that the images were re-sampled. Indeed, when the image is modelled by the bivariate cubic polynomial, the images of the intensity-curvature terms: (i) before interpolation, and (ii) after interpolation; are calculated using equations (6) and (7), respectively. When the image is modelled with the bivariate cubic Lagrange polynomial, the intensity-curvature terms: (i) before interpolation, and (ii) after interpolation; are calculated using equations (16) and (17), respectively. When the image is modelled with the bivariate linear function, the intensity-curvature terms are calculated using equations (31) and (32). The intensity-curvature terms were able to highlight and to reproduce the intensity-curvature structure of the images. Indeed, the main property of the theoretical images in Fig. 2: (a.1) light source; (a.2) sampled signal; (a.3) cross image; is to show varying pixel intensity structures. The intensity-curvature terms (b.1), (c.1), calculated from the light source image in (a.1), do reproduce the intensity-curvature image structures. Likewise the intensity-curvature terms (b.2), (c.2) (which were calculated from the sampled signal image in (a.2)) and the intensity-curvature terms (d.1), (e.1), (d.2), (e.2) do map the exponential decay of the light source image and the sampled signal image respectively. The most effective intensity-curvature image structure and detail reproduction is revealed through the intensity-curvature terms in (b.3), (c.3), (d.3) and (e.3). All of the intensity-curvature terms images presented in Fig. 2 were brightness-contrast enhanced so to reach the level of potency of the image which is capable to reproduce the image structure. The three theoretical images presented in Fig. 2(a.1), 2(a.2), 2(a.3) were also brightness-contrast enhanced in order to remove the confound factor which might be introduced in the analysis when the level of contrast enhancement is not the same for all of the images. Indeed, because of the remarkable difference between the pixel intensity values of the theoretical images and the intensity-curvature term images, the brightness-contrast enhancement cannot be set to be the same unless the potency of the images is negatively affected. Thus, the brightness-contrast enhancement of the theoretical images was adjusted to the level judged to be such to highlight the details of the image structure. Brightness-contrast enhanced theoretical images are presented in Fig. 6(b.1), 6(b.2) and 6(b.3) and the comparison with their intensity-curvature terms presented in Fig. 2, shows that the intensity-curvature structures of the theoretical images can be fairly reproduced into the intensity-curvature terms. Moreover, through the visual inspection of the theoretical images and the intensity-curvature images, is also possible to identify in the intensity-curvature term images, details of the theoretical images which are hidden into the image structures (compare for instance Fig. 2(a.3) with Fig. 2(b.3), 2(c.3), 2(d.3), 2(e.3)). Worth reporting that the properties of the intensity-curvature term images presented in this section were investigated also using 9 additional theoretical images and their behavior was found consistent with the faithful reproduction of the intensity-curvature structures.

The intensity-curvature terms of MRI images

The intensity-curvature terms are E_0 and E_{IN} [13]. Their ratio ($\Delta E = E_0 / E_{IN}$) is called intensity-curvature functional (ICF) [14].

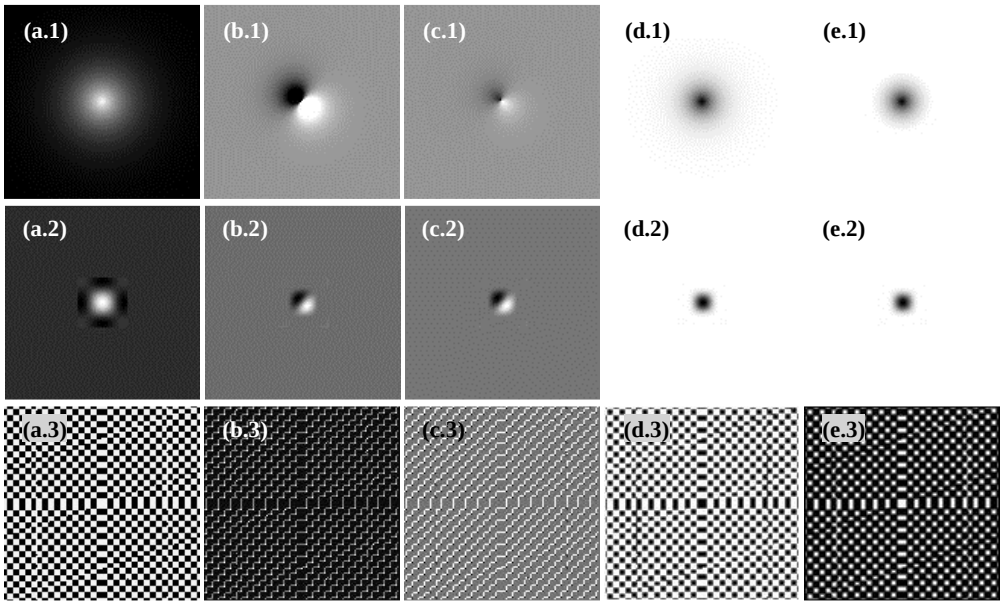

Fig. 2. Theoretical images in (a.1), (a.2) and (a.3). The intensity-curvature terms before interpolation (b.1), (b.2), and (b.3), and after interpolation (c.1), (c.2), and (c.3) were calculated using the bivariate cubic polynomial. The intensity-curvature terms before interpolation (d.1), (d.2) and (d.3), and after interpolation (e.1), (e.2) and (e.3) were calculated using the bivariate cubic Lagrange polynomial.

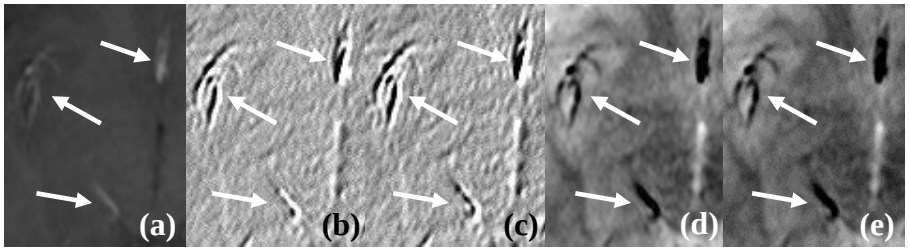

Fig. 3. (a) MRI. (b) Intensity-curvature term before interpolation E_0 of (a), calculated using the bivariate cubic polynomial. (c) Intensity-curvature term after interpolation E_{IN} of (a), calculated using the bivariate cubic polynomial. (d) Intensity-curvature term before interpolation E_0 of (a), calculated using the bivariate cubic Lagrange polynomial. (e) Intensity-curvature term after interpolation E_{IN} of (a), calculated using the bivariate cubic Lagrange polynomial.

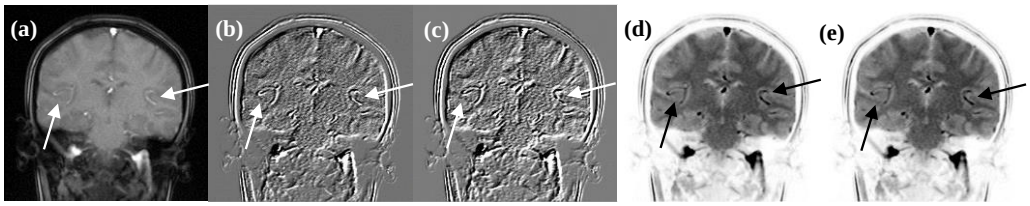

Fig. 4. MRI in (a). (b), (d) Intensity-curvature tem before interpolation E_0 of (a). (c), (e) Intensity-curvature term after interpolation E_{IN} of (a). (b), (c) were calculated when fitting the bivariate cubic model function to the MRI. (d), (e) were calculated when fitting the bivariate cubic Lagrange model function to the MRI.

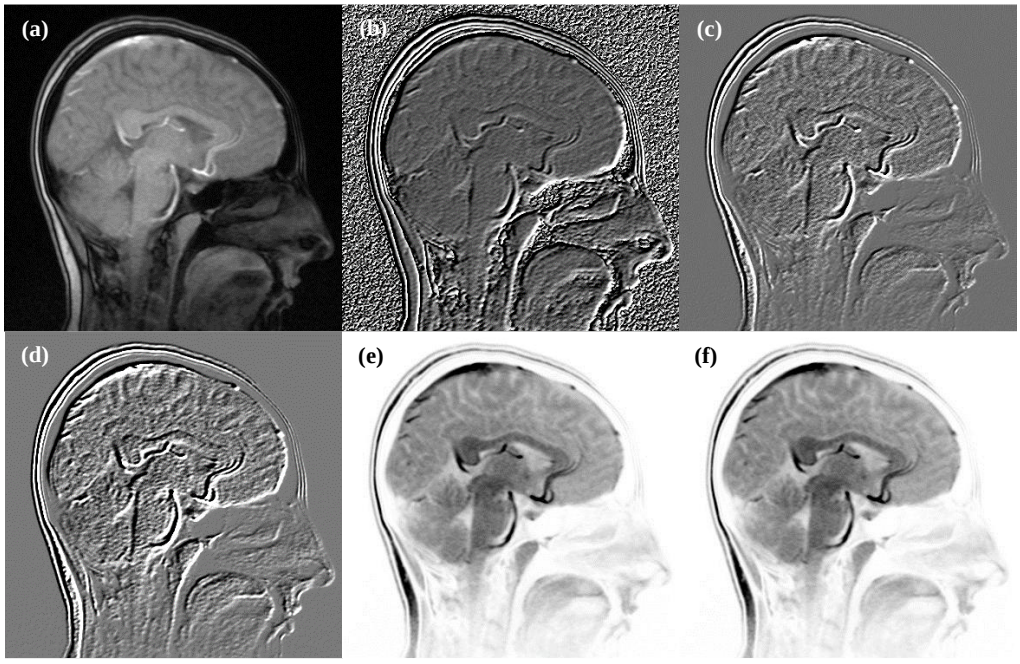

Fig. 5. (a) MRI. (b) Intensity-curvature functional calculated using the bivariate linear model function. (c), (e) Intensity-curvature terms before interpolation, and (d), (f) intensity-curvature terms after interpolation; calculated using the bivariate cubic polynomial ((c) and (d)), and the bivariate cubic Lagrange polynomial ((e) and (f)).

This section of the paper shows the characteristics of the two intensity-curvature terms with MRI applications. Fig. 3, 4 show intensity-curvature term images calculated from the MRI seen in (a). The emphasis, as indicated by the arrows, is on the highlight of selected vasculature of the human brain. Fig. 5 presents a comparison between the ICF calculated using the bivariate linear function (b), and the intensity-curvature terms calculated using the bivariate cubic polynomial ((c) and (d)), and using the bivariate cubic Lagrange polynomial ((e) and (f)). The vessels seen in the ICF (b) become prominent in the images in (c) and (d) and they change color in the images in (e) and (f).

It is due to comment on the similarity between the images in (c) and (d), and the images in (e) and (f). In such cases the ICF, which is the ratio between the two intensity-curvature terms, is a flat image without any particular significance. This means that although the formulation of the two intensity-curvature terms: before interpolation ((c) and (e)) and after interpolation ((d) and (f)) is different, the appearance of the two terms is similar and consistently their ratio is close to one ('1'), making the ICF not useful. This detail was never reported and adds value to the intensity-curvature terms of those polynomials for which the ICF is a flat image.

Study of the CC and the ICF

This section of the paper reports on the behavioral difference between the classic-curvature and the intensity-curvature functional and also presents the k-space of the two aforementioned ICMAs when they are calculated using theoretical images and MRI images.

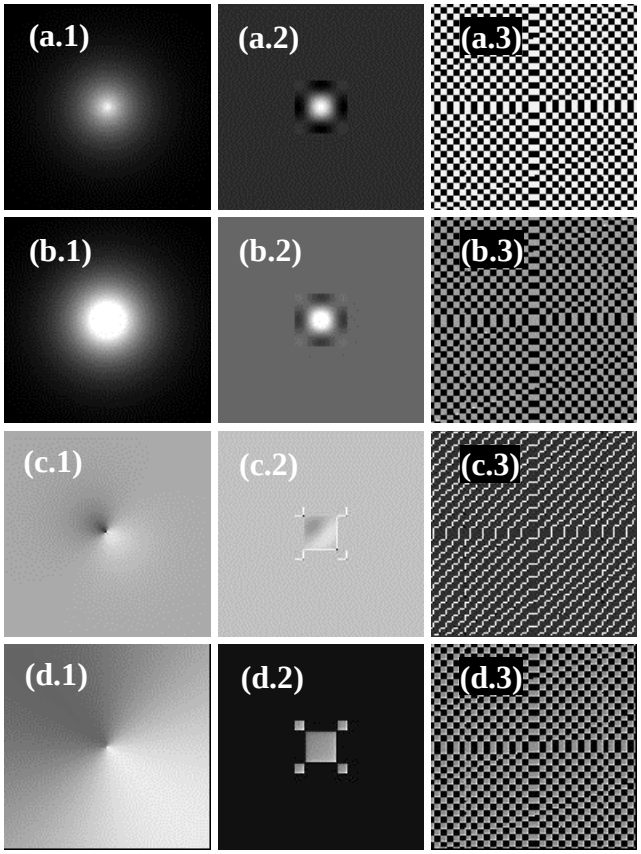

Fig. 6. Theoretical images in (a.1), (a.2) and (a.3). The three theoretical images presented in Fig. 2(a.1), 2(a.2), 2(a.3) were also brightness-contrast enhanced (see (b.1), (b.2) and (b.3)). The classic-curvature images of the theoretical images are presented in (c.1), (c.2) and (c.3), and they were calculated using the bivariate cubic polynomial. The intensity-curvature images of the theoretical images are presented in (d.1), (d.2) and (d.3), and they were calculated using the bivariate linear model function.

The effect of combining together the intensity of the signal with the second order partial derivatives of the model function fitted to the signal is illustrated in Fig. 6(c.1), 6(c.2), 6(c.3) (classic-curvature images) and Fig. 6(d.1), 6(d.2), 6(d.3) (intensity-curvature functional images). The classic-curvature images highlight the details of the theoretical images, whereas the intensity-curvature functional images present the same behavior and, in addition to it, they sharpen the details of the theoretical images. Recent research [11] reports the empirical evidence that both the classic-curvature and the intensity-curvature functional are suggested to be high pass filtered signals when calculated while fitting to the MRI images the bivariate cubic polynomial and the bivariate linear function (see equations (5) and (34) respectively). Fig. 7 shows the k-space of the two aforementioned ICMAs and presents the evidence that the Fourier properties of the CC and the ICF are different, as shown in Fig. 7(e), 7(f), 7(g) (k-space of the CC images presented in Fig. 6(a.1), 6(a.2), 6(a.3) respectively) and in Fig. 7(h), 7(i), 7(j) (k-space of the ICF images presented in Fig. 6(d.1),

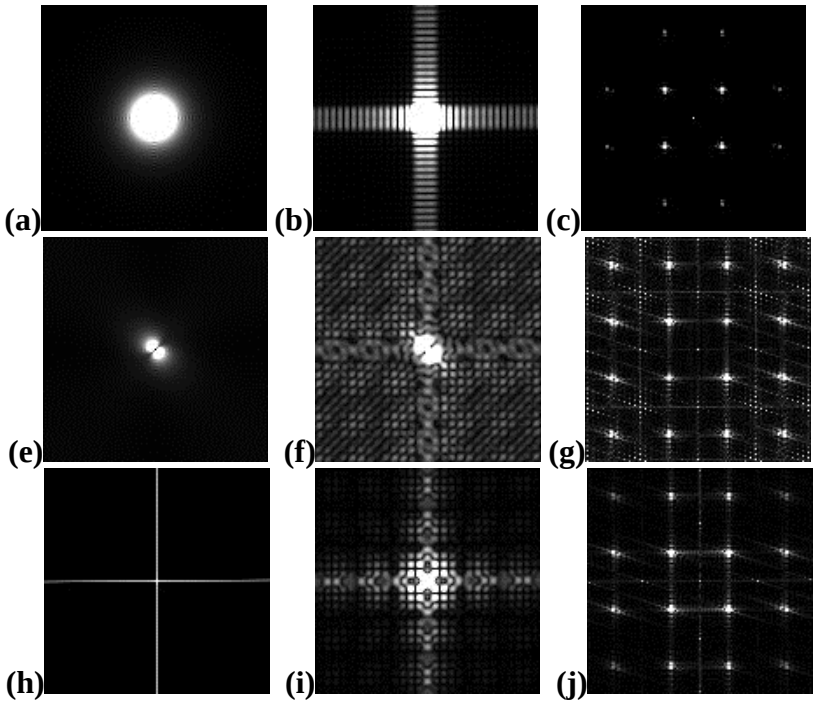

Fig. 7. (a), (b), (c) K-space of the theoretical images presented in Fig. 2(a.1), 2(a.2) and 2(a.3) respectively. (e), (f), (g) K-space of the classic-curvature images presented in Fig. 6(c.1), 6(c.2) and 6(c.3) respectively. (h), (i), (j) K-space of the intensity-curvature functional images presented in Fig. 6(d.1), 6(d.2) and 6(d.3) respectively.

6(d.2), 6(d.3) respectively). In addition, the CC and the ICF images have Fourier properties different from those of the high pass filtered signal. Indeed, when comparing the k-space of the MRI high pass filtered signal (see Fig. 8(f), 8(l)) to the k-space of the CC of the MRI signal (see Fig. 8(e)) and the k-space of the ICF of the MRI signal (see Fig. 8(k)), it is possible to discern that the CC and the ICF are not the same as high pass filtered signals.

The filtering properties of the CC and the ICF

It is possible to treat the classic-curvature images and the intensity-curvature functional images as filter masks [11]. Fig. 9 shows the MRI in (a), the CC of the MRI in (b), the ICF of the MRI in (c), the result of the convolution between the MRI and the CC in (d), and the result of the convolution between the MRI and the ICF in (e). The images in (d) and (e), in Fig. 9, likewise presented in Fig. 10, show the filtering capabilities of the CC and the ICF images. In Fig. 9 the emphasis is on the vasculature of the human brain, whereas in Fig. 10 the emphasis is on the human brain cortex. The use of the classic-curvature and the intensity-curvature functional as filter masks makes it possible to filter the MRI so to observe details of interest and to suppress what is not the object of study. As an example of the aforementioned usage, Fig. 9(d) and Fig. 9(e) highlight the human brain vasculature. The vessels seen in dark color inside the ellipses in Fig. 9(d) and 9(e) can also be seen in the CC image in (b) and in the ICF image in (c),

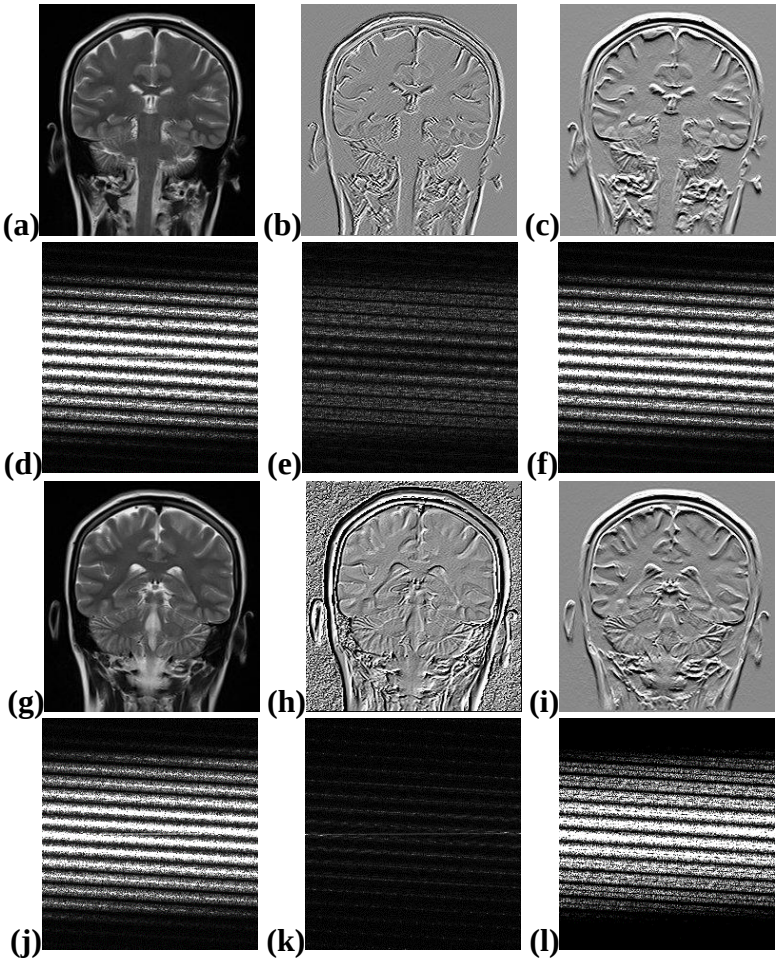

Fig. 8. (a), (g) T2-weighted MRI images. (b) Classic-curvature of (a). The MRI images in (a) and (g) are high pass filtered and presented in (c) and (i) respectively. (d), (e) and (f) Are the k-space magnitude images of (a), (b) and (c) respectively. (h) Intensity-curvature functional of (g). (j), (k) and (l) Are the k-space magnitude images of (g), (h) and (i) respectively.

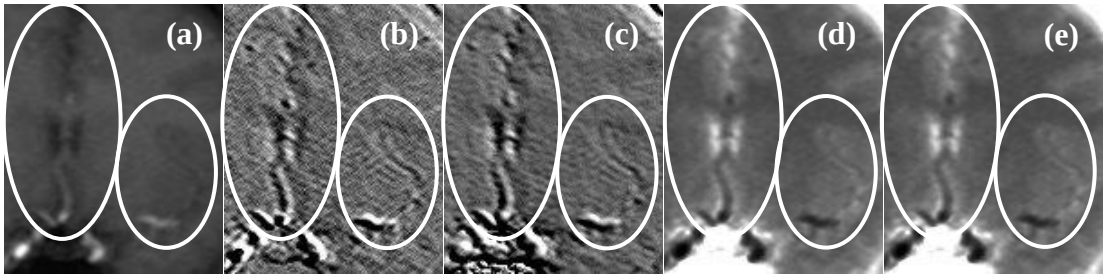

Fig. 9. (a) MRI image. (b) Classic-curvature of (a) calculated using the bivariate cubic polynomial. (c) ICF of (a) calculated using the bivariate linear function. (d) Result of the convolution of the MRI with the image in (b). (e) Result of the convolution of the MRI with the image in (c). The highlight of the pictures is on samples of the vasculature of the human brain (see vessels inside the ellipses).

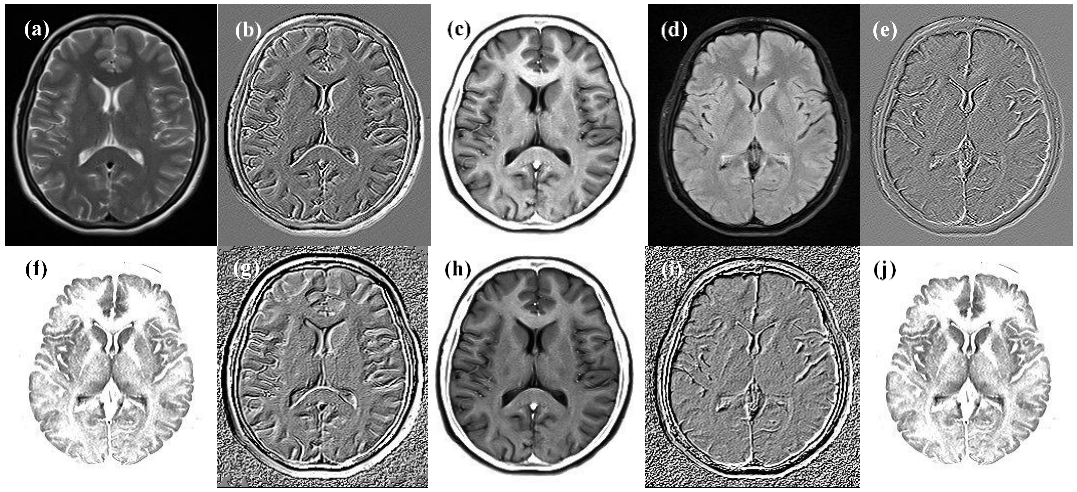

Fig. 10. (a) T2-weighted MRI image. (b) Classic-curvature of (a). (c) Result of the convolution of the T2-weighted MRI with the image in (b). (d) FLAIR MRI. (e) Classic-Curvature of (d). (f) Result of the convolution of the FLAIR MRI with the image in (e). (g) Intensity-curvature functional of the T2-weighted MRI in (a). (h) Result of the convolution of the T2-weighted MRI with the image in (g). (i) Intensity-curvature functional of the FLAIR MRI image in (d). (j) Result of the convolution of the FLAIR MRI with the image in (i).

however they do not appear distinct from the rest of the brain matter as they appear in the filtered images shown in (d) and (e). In Fig. 9(d) and 9(e) is also observable clear and neat distinction between gray and white matter of the cortex. Fig. 10(c), 10(f), 10(h), and 10(j) highlight the human brain cortex. There are differences visible in the four aforementioned pictures. The CC (b) and the ICF (g) of the T2-weighted MRI filter out to the images in (c) and (h) respectively. In (c) and (h) it is possible to discern clearly the structure of the human cortex, gray and white matter, the sulci and the gyri, and the ventricles. The CC (e) and the ICF (i) of the FLAIR MRI filter out to the images in (f) and (j), respectively. And in such images the emphasis is on the distinction between gray

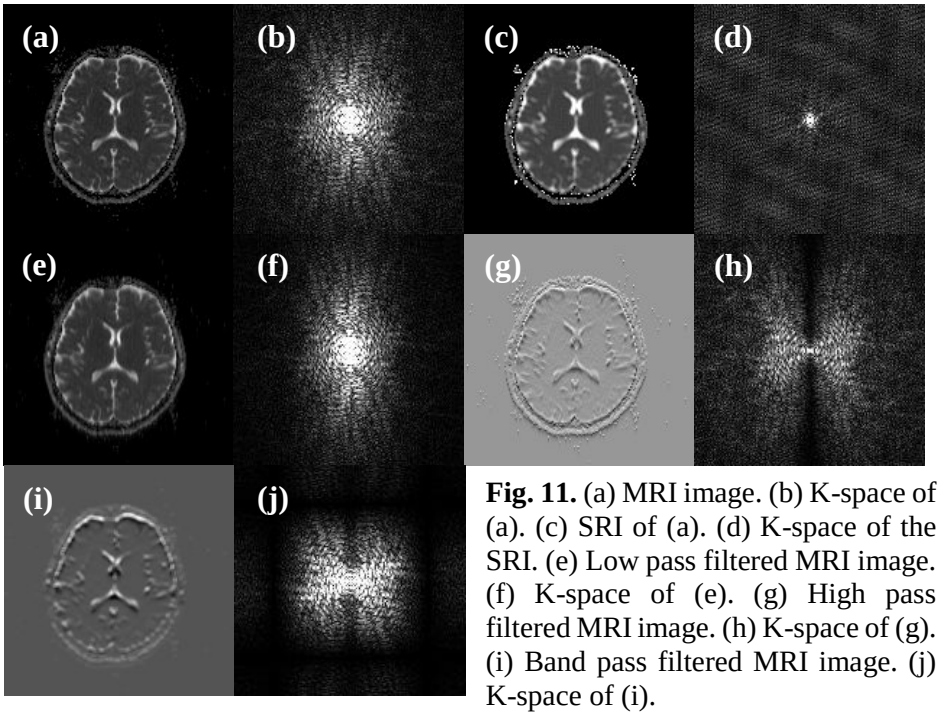

Fig. 11. (a) MRI image. (b) K-space of (a). (c) SRI of (a). (d) K-space of the SRI. (e) Low pass filtered MRI image. (f) K-space of (e). (g) High pass filtered MRI image. (h) K-space of (g). (i) Band pass filtered MRI image. (j) K-space of (i).

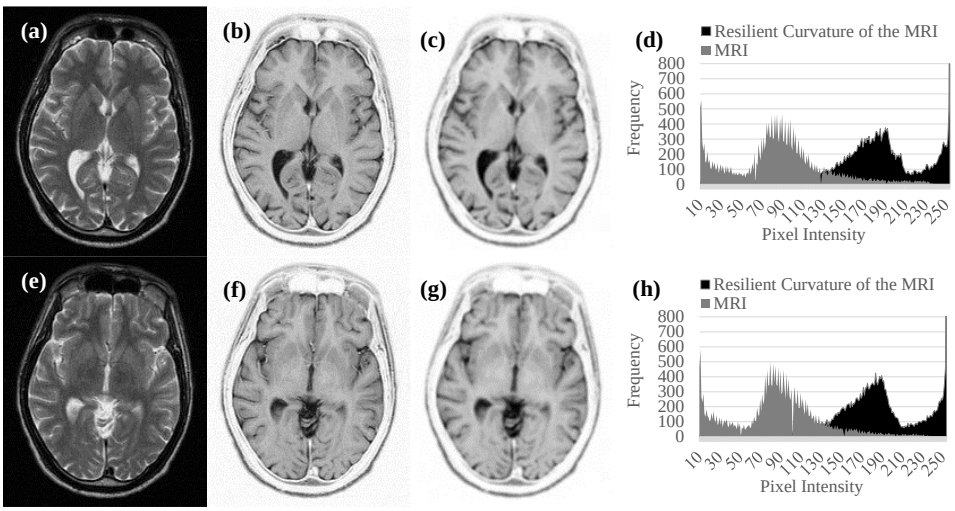

Fig. 12. T2-weighted MRI in (a) and (e). The inverted MRI is in (b) and (f) so to show the main characteristic of the resilient curvature which is to invert the gray scale of the image, to smooth the image and also to magnify the gray scale of the image (see (c) and (g)). The histograms of the frequency distribution of the MRI and the resilient curvature are presented in (d) and (h) and they show that the resilient curvature is not the exact mirrored opposite of the MRI.

and white matter, although sulci, gyri and ventricles are still distinguishable. In MRI tumor studies we have observed that the FLAIR MRI, when filtered with the CC and the ICF, presents details of the tumor with finer level of details, which cannot be otherwise observed [15].

The signal resilient to interpolation (SRI) and the resilient curvature (RC)

Fig. 11 shows the comparison of the MRI images versus the filtered images, the filtered images versus the SRI images, and additionally, the K-space of each of the three filters versus the K-space of the SRI. Through visual inspection of the data presented in the pictures, it can be inferred that the SRI is also a filter [12] (see the smoothing in (c) versus the smoothing in (e), which is a low pass filtered image). Fig. 12 shows the main property of the resilient curvature which is to smooth, invert and magnify the gray scale of the MRI [12].

Discussion

Image intensity based MRI processing includes Deformation-based Morphometry (DBM) [17] and Voxel-based Morphometry (VBM) [18] methods. DBM and VBM were used to extract features from Alzheimer MRI data [19] provided by the OASIS dataset [20]. Voxel-based Morphometry feature extraction was found to be best performing when compared to a large array of algorithms within the context of the diagnosis of dementia from MRI [21]. Edge detection of human brain MRI structures is another area of application of image intensity based methods which use filtering techniques [22], and it is a preprocessing technique within the context of MRI image feature extraction [23]. Region growing techniques combined with shape based difference images were used to extract features from Magnetic Resonance Angiography [24]. Segmentation is another area of MRI research which uses image intensity based algorithms, region growing algorithms and morphological operators for the extraction of human brain structures [25]. Other segmentation applications include: (i) an algorithm for the measurement and the extraction of the hippocampus from human brain MRI images [26]; (ii) a genetic algorithm search which is used to gather the features for the representation of human brain MRI tumor data [27]. As can be seen from the literature, the intensity-curvature terms are original techniques. And, as shown in this paper, the intensity-curvature terms are able to perform feature extraction as well as to set the grounding theory for the calculation of the ICMAs. The ICMAs are image re-sampling techniques which depend on the second order partial derivatives of the image. The methodological approach is mathematically well defined because the calculation of the second order partial derivatives of the image is performed once a model function is fitted to the image on a pixel-by-pixel basis [28]. The literature offers several methods of calculation of the derivatives of an image: the Sobel operator [29], compact finite differences [30], and gradient operators [31]. The benefits of fitting a polynomial model to the image data [28] are immediately granted by the variety of re-sampling techniques that are made available [14]. What can be argued, though, is that model fitting is arbitrary. Thus, the effort of this paper is geared towards the presentation of results obtained modelling the image data with three different polynomial functions. The implications, the novelty and the contribution provided by this paper shall be discussed in the next sections.

The implications of the intensity-curvature terms

The idea of the intensity-curvature terms in image processing is to map the image intensity to the image intensity-curvature. The intensity-curvature content of the image is characterized through the image processing technique that merges the pixel intensity of an image with the sum of second order partial derivatives (the classic-

curvature) of the model function fitted to the image data. The technique is able to extract features from the images and this has been studied in this paper through the use of theoretical images and MRI images of the human brain. The results indicate that the intensity-curvature terms are able to highlight and reproduce the intensity-curvature structure of the images as well as to extract vasculature features from the human brain MRI images. Following the inception of the intensity-curvature terms, this paper reports another of their implications, which is that of the feasibility to extend the mathematical procedure up to the calculation of three additional intensity-curvature measurement approaches (ICMAs). The ICMAs are: (i) the intensity-curvature functional (ICF), (ii) the signal resilient to interpolation (SRI), and (iii) the resilient curvature (RC). The intensity-curvature functional has been studied within the context of the tumor contour line detection [16], and it was later suggested to be a high pass filtered signal [11]. This paper clarifies that the CC, the ICF and the high pass filtered signal are not the same because of the difference existing between the k-space of the CC, the k-space of the ICF, and the k-space of the high pass filtered signal. The signal resilient to interpolation and the resilient curvature have been studied and characterized within the context of the study of human brain MRI images [12]. This paper summarizes and confirms earlier findings [12] which define the signal resilient to interpolation as an alternative filter. And this paper also confirms the properties of the resilient curvature as an alternative image inversion technique which moreover smooths and magnifies the gray scale of the image.

The novelty

The novelty reported in this paper is to report for the first time the behavior of the intensity-curvature terms calculated when the bivariate cubic polynomial and the bivariate cubic Lagrange polynomial are fitted as model functions to the image data. The behavior was studied on theoretical images and it was found that the intensity-curvature terms of the two aforementioned model polynomial functions allow the reproduction of the intensity-curvature structure and structural details of the theoretical images (see Fig. 2). An additional novelty is presented in Fig. 7, 8, where it is shown that the Fourier properties of the classic-curvature and the intensity-curvature functional are different, and they are also different when compared to the Fourier properties of the high pass filtered signal. Samples of the vasculature of the human brain MRI [32] have been studied in Fig. 3, 4, 5, 9, and the results show that the intensity-curvature terms can highlight the vasculature. Additionally, the results obtained convolving the MRI with the CC and the ICF images, in Fig. 10, confirm the filtering capabilities of the two aforementioned ICMAs. Overall, the contribution to image processing is the characterization of the intensity-curvature structure of an image which is possible through the calculation of the intensity-curvature terms. Finally, the procedural and methodological contribution of the paper is the extension of the mathematical procedure to the calculation of three ICMAs: (i) the intensity-curvature functional, (ii) the signal resilient to interpolation and (iii) the resilient curvature; which are found to have useful signal processing characteristics.

Conclusion

The intensity-curvature terms are able to characterize the reproduction of the image structure and the image details of theoretical images. And, also to highlight the vasculature of the human brain from MRI images. The role of the intensity-curvature term in image processing of the human brain MRI is to make it possible to calculate the ICF, the SRI and the RC images, and also the two intensity-curvature term images. Therefore, the intensity-curvature term is the

foundation of five imaging domains, where it is possible to collect complementary and/or additional information about the MRI of the human brain anatomy and structure, and also to perform feature extraction.

References

[1] Zacharaki EI, Wang S, Chawla S, Soo Yoo D, Wolf R, Melhem ER, Davatzikos C. Classification of brain tumor type and grade using MRI texture and shape in a machine learning scheme. Mag Reson Med 2009;62(6):1609-18.

[2] Van Herk M, Kooy HM. Automatic three-dimensional correlation of CT-CT, CT-MRI, and CT-SPECT using chamfer matching. Med Phys 1994;21(7):1163-7.

[3] García-Sebastián M, Savio A, Graña M, Villanúa J. On the use of morphometry based features for Alzheimer's disease detection on MRI. In: Bio-Inspired Systems: Computational and Ambient Intelligence, Berlin: Springer; 2009. p. 957-64.

[4] Awate SP, Zhang H, Gee JC. A fuzzy, nonparametric segmentation framework for DTI and MRI analysis: with applications to DTI-tract extraction. IEEE Trans Med Imaging 2007;26(11):1525-36.

[5] Magnin B, Mesrob L, Kinkingnéhun S, Pélégrini-Issac M, Colliot O, Sarazin M, Dubois B, Lehéricy S, Benali H. Support vector machine-based classification of Alzheimer's disease from whole-brain anatomical MRI. Neuroradiology 2009;51(2):73-83.

[6] Rex DE, Shattuck DW, Woods RP, Narr KL, Luders E, Rehm K, Stolzner SE, Rottenberg DA, Toga AW. A meta-algorithm for brain extraction in MRI. Neuroimage 2004;23(2):625-37.

[7] El-Dahshan ES, Hosny T, Salem AB. Hybrid intelligent techniques for MRI brain images classification. Digit Signal Process 2010;20(2): 433-41.

[8] Zhang Y, Dong Z, Wu L, Wang S. A hybrid method for MRI brain image classification. Expert Syst Appl 2011;38(8):10049-53.

[9] Zhou X, Wang S, Xu W, Ji G, Phillips P, Sun P, Zhang Y. Detection of pathological brain in MRI scanning based on wavelet-entropy and naive bayes classifier. In: Bioinformatics and biomedical engineering, Springer; 2015, p. 201-9.

[10] Ciulla C, Veljanovski D, Rechkoska SU, Risteski FA. Intensity-curvature measurement approaches for the diagnosis of magnetic resonance Imaging brain tumors. J Adv Res 2015;6(6):1045-69.

[11] Ciulla C, Veljanovski D, Rechkoska SU, Risteski FA. On the properties of the intensity-curvature measurement approaches: the classic-curvature and the intensity-curvature functional. J Solid Tumors 2016;6(1): 38-53.

[12] Ciulla C, Veljanovski D, Rechkoska SU, Risteski FA. On the properties of the intensity-curvature measurement approaches: The signal resilient to interpolation and the resilient curvature. IJICA 2016;7(2):91-118.

[13] Ciulla C, Deek FP, On the approximate nature of the bivariate linear interpolation function: A novel scheme based on intensity-curvature. ICGST - International Journal on Graphics, Vision and Image Processing 2005;5(7):9-19.

[14] Ciulla C. Signal resilient to interpolation: An exploration on the approximation properties of the mathematical functions. CreateSpace Publisher; 2012.

[15] Ciulla C, Veljanovski D, Risteski FA, Rechkoska SU. On the filtering properties of classic-curvature and intensity-curvature functional images: Applications in magnetic resonance imaging. IJAPR 2016;3(1):77-98.

[16] Ciulla C, Rechkoska SU, Capeska Bogatinoska D, Risteski FA, Veljanovski D. On the intensity-curvature functional of the bivariate linear function: The third dimension of magnetic resonance 2D images in a tumor case study. American Journal of Signal Processing 2014;4(2):41-8.

[17] Chung MK, Worsley KJ, Paus T, Cherif C, Collins DL, Giedd JN, Rapoport JL, Evans AC. A unified statistical approach to deformation-based morphometry. Neuroimage 2001;14(3):595-606.

[18] Ashburner J, Friston KJ. Voxel-based morphometry - the methods. Neuroimage 2000;11(6):805-21.

[19] Papakostas GA, Savio A, Graña M, Kaburlasos VG. A lattice computing approach to Alzheimer's disease computer assisted diagnosis based on MRI data. Neurocomputing 2015;150: 37-42.

[20] Marcus DS, Wang TH, Parker J, Csernansky JG, Morris JC, Buckner RL. Open access series of imaging studies (OASIS): cross-sectional MRI data in young, middle aged, nondemented, and demented older adults. J Cognitive Neurosci 2007;19(9):1498-507.

[21] Bron EE, Smits M, Van Der Flier WM, Vrenken H, Barkhof F, Scheltens P, Papma JM, Steketee RM, Orellana CM, Meijboom R, Pinto M. Standardized evaluation of algorithms for computer-aided diagnosis of dementia based on structural MRI: The CAD-Dementia challenge, Neuroimage 2015;1:562-79.

[22] Udomhunsakul S, Wongsita P. Feature extraction in medical MRI images. In: Cybernetics and Intelligent Systems, IEEE Conference Vol. 1, 2004. p. 340-4.

[23] Rezai-Rad G, Aghababaie M. Comparison of SUSAN and Sobel edge detection in MRI images for feature extraction. In: Information and Communication Technologies, ICTTA'06, 2nd IEEE Vol. 1, 2006. p. 1103-07.

[24] Arimura H, Li Q, Korogi Y, Hirai T, Katsuragawa S, Yamashita Y, Tsuchiya K, Doi K. Computerized detection of intracranial aneurysms for three-dimensional MR angiography: Feature extraction of small protrusions based on a shape-based difference image technique. Med Phys 2006;33(2):394-401.

[25] Freeborough PA, Fox NC, Kitney RI. Interactive algorithms for the segmentation and quantitation of 3-D MRI brain scans. Computer Methods and Programs in Biomedicine 1997;53(1):15-25.

[26] Ashton EA, Parker KJ, Berg MJ, Chen CW. A novel volumetric feature extraction technique with applications to MR images. IEEE Transactions on Medical Imaging 1997;16(4):365-371.

[27] Velthuizen RP, Hall LO, Clarke LP. Feature extraction for MRI segmentation. J Neuroimaging 1999;9(2):85-90.

[28] Haralick RM. Digital step edges from zero crossing of second directional derivatives. IEEE TPAMI, Vol. PAMI-6, No. 1, pp. 58-68, 1984.

[29] Cha Y, Kim S. The error-amended sharp edge (EASE) scheme for image zooming. IEEE Transactions on Image Processing 2007;16(6):1496-1505.

[30] Lele SK. Compact difference schemes with spectral-like resolution. J Comput Phys 1992;103:16-42.

[31] Farid H, Simoncelli EP. Differen tiation of discrete multidimensional signals. IEEE Transactions on Image Processing 2004;13(4):496-508.

[32] Haacke EM, Xu Y, Cheng Y-C, Reichenbach JR. Susceptibility Weighted Imaging (SWI). Mag Reson Med 2004;52:612-8.